Surface Plasmonic Nano Grating for Improved the Responses of GaAs PIN photodetectors

Nada AbdElaziz
Delta Higher Institute for engineering and technology
Bedir Bedir yousif (bedir.yousif@gmail.com)
Kafrelsheikh University Faculty of Engineering https://orcid.org/0000-0002-3217-1555
Eman AbdElhalim
Mansoura University Faculty of Engineering
Waleed Gaballah
Mansoura Higher Institute for engineering and technology
Ahmed Samra
Mansoura University Faculty of Engineering

Research Article

Keywords: Plasmonics, Nano grating, GaAs photodetectors, Surface plasmon polaritons

Posted Date: March 24th, 2022

DOI: https://doi.org/10.21203/rs.3.rs-1432169/v1

Surface Plasmonic Nano Grating for Improved the Responses of GaAs PIN photodetectors

Nada AbdElaziz[1*], Bedir Yousif[2,3], Eman AbdElhalim[4a], Waleed M. Gaballah[5], Ahmed S. Samra [4b]**

[1]Electronics and Communications Department, Delta Higher Institute for Engineering and Technology, Delta Academy, Mansoura, Egypt.

Email: engnada3112@gmail.com

[2]Electrical Engineering Department, Faculty of Engineering, Kafrelsheikh University, Kafrelsheikh 33516, Egypt.
Email: bedir.yousif@gmail.com and bedir.yousif@eng.kfs.edu.eg

[3] Electrical Engineering Department, Faculty of Engineering and Information Technology, Onaizah Colleges, Al Qassim, Saudi Arabia.
Email: bedir.yousif@oc.edu.sa

[4a]Electronics and communications Department, Faculty of Engineering, Mansoura University, Mansoura 35516, Egypt.

Email: eman_haleim@mans.edu.eg

[5]Electronics and Communications Engineering Department Mansoura Higher Institution for Engineering and Technology.

Email: w_gaballa@hotmail.com
[4b] Electronics and communications Department, Faculty of Engineering, Mansoura University, Mansoura 35516, Egypt.
Email: ahsamra@yahoo.co.uk

Address correspondence to E-mail: bedir.yousif@gmail.com; engnada3112@gmail.com

Abstract

The photonics world is becoming increasingly interested in plasmonic photodetectors. The field of plasmonics allows light to be dedicated into small spaces in metallic structures, and this property has the ability to simulate extra improvements in performance of photodetectors. In this work it is presented gold (Au) and Aluminum (Al) surface plasmon polariton (SPP) GaAs PIN photodetector achieved higher internal quantum efficiency (IQE), as the IQE with Au and Al SPP rectangle grating is 95.01%, while the IQE with Au SPP rectangle grating is 85%, which indicates an improvement of 10.01%. It is also presented nanograting various shapes such as triangular, ellipse, bowtie and circle, and investigate its impact on improving the performance of the proposed photodetector. The internal quantum efficiency is improved to 98.48 % with a total enhancement IQE of 13.48%. Moreover, output current and responsivity are improved. This remarkable enhancement is achieved with bowtie grating as compared to other shapes and previous published papers.

Keywords

Plasmonics, Nano grating, GaAs photodetectors, Surface plasmon polaritons.

1. Introduction

One of the most essential optoelectronic information devices are photodetectors. The most important factors for photodetector designs are Integration density, sensitivity, operating range of wavelengths, speed, affordability, and multifunctionality are all important considerations (such as polarization, wavelength, and chirality detection). Novel photodetector designs and research are generated by new materials and mechanisms [1, 3]. SPP (Surface plasmon polariton) technology has demonstrated a remarkable promise in the development of active GaAs PIN circuits. Plasmonics has provided a significant reduction in terms of photonic component size by taking advantage of metals' capacity to confine light at the deep-subwavelength dimension [2- 8]. developing technology in the direction of minimizing the integration of electronic and optical components [8]. Which opens the path in preparation for the next generation of very dense interconnects [4], which will have integrated optoelectronic interfaces. Metallic elements are naturally found in plasmonic photodetectors. Such elements can play one of two kinds: (1) Metals have the potential to be used in hot-carrier devices as the absorber (2) Metals can improve the

electromagnetic field within an absorber. Fig.1 illustrates a graphical representation of classification for plasmonic photodetectors. First, we distinguish between photodetectors that use semiconductors or metals as an absorber (hot-carrier photodetectors). The photodetectors are then classified into one of the four basic methods of operation: The photoconductor detector, the P-I-N detector, the tunnel-junction, and the Schottky-detector. Schottky and tunnel-junction detectors are used in plasmonic hot-carrier detectors operating techniques. Finally, there are three fundamental forms of plasmonics enhancement that can be applied to each detector type: a localized plasmon polariton in a metallic nanoparticle, a surface plasmonic polariton (SPP) in a waveguide, or a grating type plasmon, that plasmonic field enhancement techniques can be used in photodetectors, including semiconductor and hot-carrier to increase efficiency [5, 6].

The free electrons collective oscillations in metallic nanostructures are well-known as plasmons After plasmons decay. The multifunctional detection capabilities of plasmonic structures, like polarization, wavelength, and chirality detecting [7] are further benefits of plasmon enhanced photodetection. Plasmons can be used to improve light absorption in materials in addition to the hot carrier injection technique [9]. Plasmon enhanced photodetectors were examined [10].as well as recently demonstrated in semiconductors [11, 12] and graphene [13- 15].

Light is thought to be among the brightest possibilities for the purpose of substituting signals generated by electronic devices (as information carriers). However, one of the fundamental drawbacks in integrated circuits and the devices of optical signal processing using electromagnetic waves as carriers of information is the availability of a minimum level of integration and downsizing, which is significantly below that of current electronics. Light diffraction limit in dielectric medium causes this problem, since it prevents electromagnetic waves from being localized into nanoscale areas with wavelengths far less than the wavelength of light for substance [16].

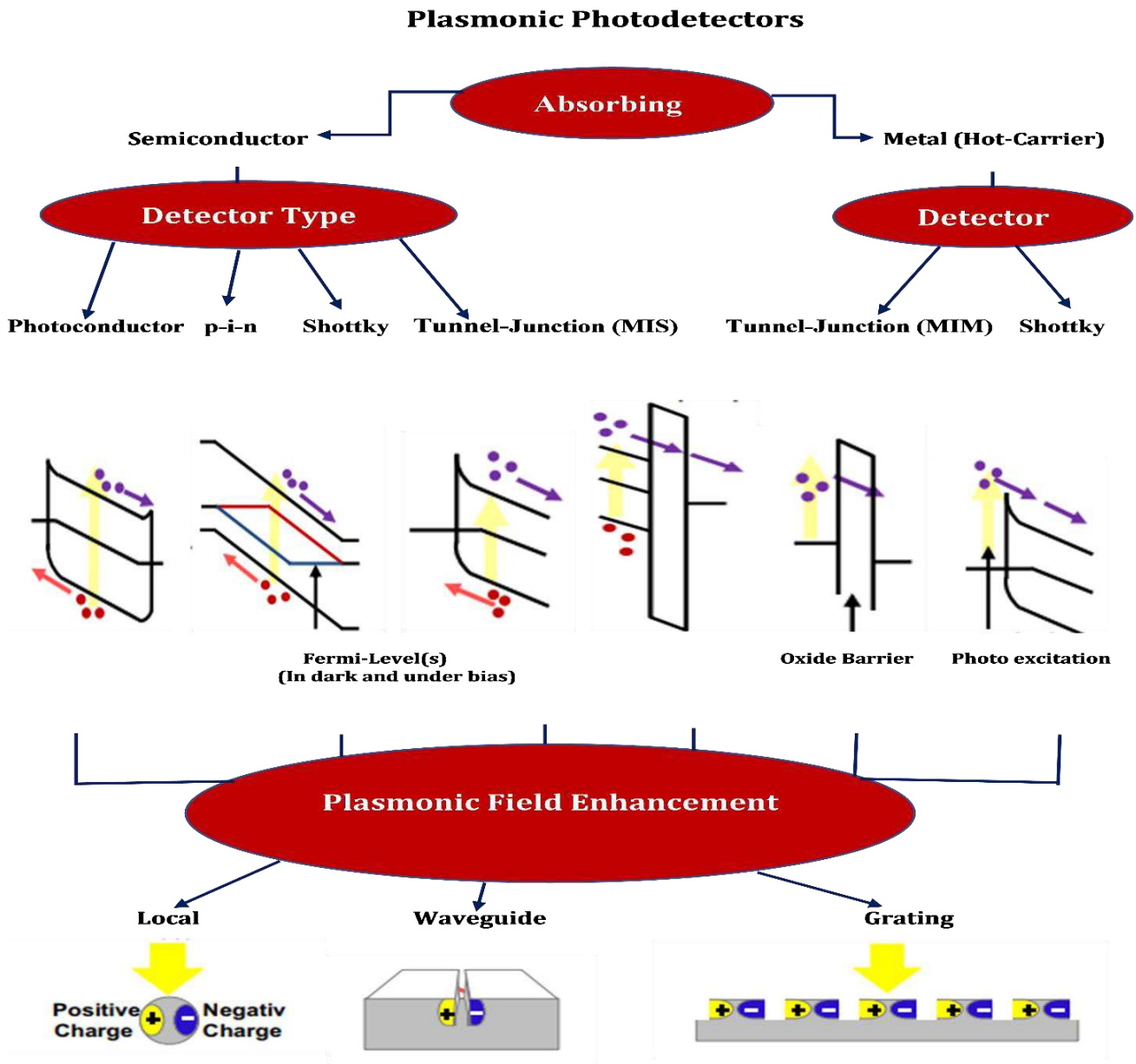

Fig.1: classification of plasmonic photodetectors.

Among the practical techniques of evading the diffraction limit and achieving localization of electromagnetic energy (at optical frequencies) into nanoscale regions as tiny as a few nanometers is to use negative dielectric permittivity substances. Metals with a frequency below that of plasma are the most commonly available materials for this purpose. Surface plasmon–polariton (SPP) modes are

known to be guided by metal structures and interfaces [17]. In the metal, Electromagnetic waves are connected to electron plasma collective oscillations.

Electromagnetic waves in the metal are related to electron plasma aggregate oscillations. As a result, plasmonics is a branch of nanophononics that studies the transmission, localization, and steering of extremely confined SPP modes utilizing metallic nanoscales beyond the diffraction limit. The allure of combining the compactness of an electronics with the bandwidth of a photonics has fueled the explosive growth of plasmonic waveguides whose mode confinement is not limited by the guiding structure's material properties [18]. Several other studies have been conducted on metallic nanoparticles for their many uses, including optoelectronics, medicinal applications, energy-based research, sensors, and diagnostics [19].

On this photodetector, it is employed tools of COMSOL and MATLAB. Adding gold and aluminum SPPs (surface plasmon polaritons) to a photodetector's top with PIN type with various shapes of grating like rectangular, triangular, ellipse, bowtie and circle boosted output photocurrent, IQE (internal quantum efficiency), and responsivity, according to the study.

The remaining sections of the paper are organized as follows: The structure of the proposed PIN photodetector, as well as its parameter values, are presented in Section 2. The SPP Mathematical Modeling utilized in this study is detailed in Section 3. Section 4 explains the simulation's results. at last, Section 5 discusses the study's conclusion.

2. Design Structure

The device structure designed and prepared in this paper is depicted in Fig. 2 (a–e). The photodetector with GaAs PIN type is modeled utilizing Gold and Aluminum as (surface plasmon polaritons) SPP layers on the photodetector's surface in this proposed structure. GaAs was used as the active material. Gold and Aluminum SPP layers were built on the model's top, with a gold P connector and a silver N connector to identify that the current is flowing across the photodetector when the light state is generated. Table 1 contains more information about the model. Nanograting various shapes SPP layers such as rectangular, triangular, ellipse, bowtie and circle are designed to study its impact on improving the performance of the proposed PIN photodetector.

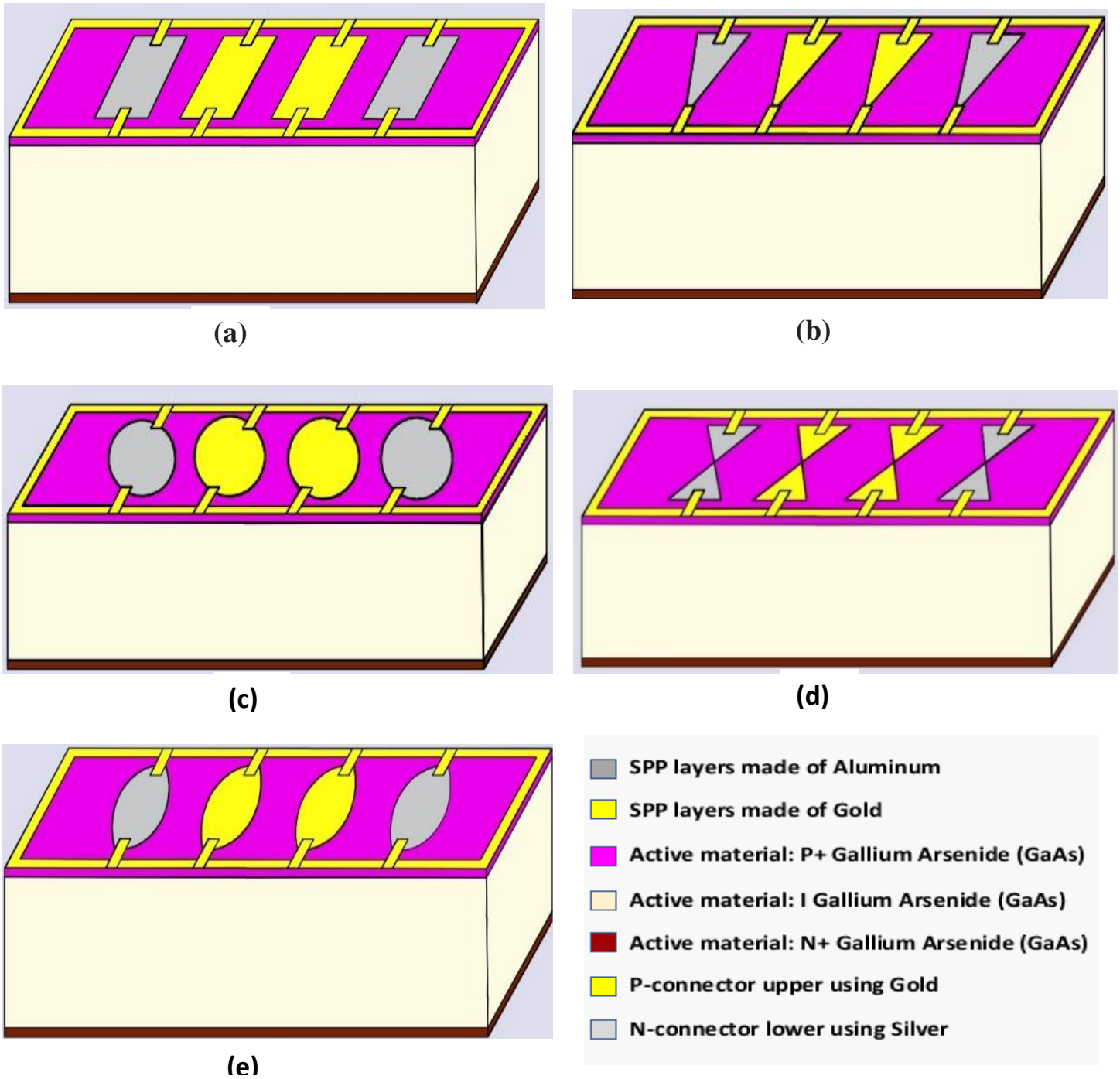

Fig.2: PIN photodetector made of GaAs with gold and aluminum SPP (a) rectangular, (b) triangular, (c) circle, (d) bowtie, and (e) ellipse grating.

The sloping nature of the conduction and valence bands, which have the highest energy at the p-contact and the lowest at the n-contact, makes the PIN structure effective for photodiode devices. Which designed to operate in reverse bias, Because the absorbed light

is utilized to generate current, this is also known as photoconductive mode as one of the operating modes.

Table 1 Model parameters used in computations.

Parameters	Values
Input power	1000 1000 (W/m^2)
Voltage across the N-contact	2 (V)
Voltage across the P-contact	0 (V)
GaAs refractive index (real component)	3.5
Thickness of the Detector	1 (um)
Doping of Anode (P+ doping)	$1e^{21}$ (atom/cm^3)
Doping of Cathode (N+ doping)	$1e^{21}$ (atom/cm^3)
Thickness of anode doping	100 (nm)
Thickness of Cathode doping	100 (nm)
width of Au SPP slice	500 (nm)
width of Al SPP slice	500 (nm)
Au SPP slice thickness	3.7 (nm)
Al SPP slice thickness	3.7 (nm)

3. SPP Mathematical Modeling

3.1 SPP Excitation

Both electrons and photons can excite SPPs. Electron excitation is achieved by firing electrons into a metal's bulk [20]. Vector of scattering transfers energy to the plasma's bulk. When one of the scattering vector components is parallel with the surface, a surface plasmon polariton forms [21].

Both the frequency and momentum of the photon and the SPP must be the same for it to excite the SPP. Free-space photons, on the other hand, have less momentum than SPPs for a given frequency because their dispersion relations are different (see below). A free-space photon coming from air cannot be paired directly to an SPP because of this momentum imbalance. An SPP on a smooth metal's surface, for the same reason, cannot emit energy into the dielectric as a free-space photon dielectric (if the dielectric is uniform). This mismatch is similar to the transmission loss that occurs during total internal reflection.

3.2 Fields and Dispersion Relation of SPP

To determine the characteristics of an SPP, utilize Maxwell's equations. The metal–dielectric contact is represented as the $z = 0$ plane, with the metal at $z < 0$ and with the dielectric at $z > 0$ in this coordinate system. Both the magnetic and electric fields are shown as a function of (x, y, z, t) [17, 22]:

$$E_{x,n}(x, y, z, t) = E_0 e^{ik_x x + ik_{z,n}|z| - i\omega t} \quad (1)$$

$$E_{z,n}(x, y, z, t) = \pm E_0 \frac{k_z}{k_{z,n}} e^{ik_z x + ik_{z,n}|z| - i\omega t} \quad (2)$$

$$H_{y,n}(x, y, z, t) = H_0 e^{ik_x x + ik_{z,n}|z| - i\omega t} \quad (3)$$

Where,

- The kind of substance is denoted by $\boldsymbol{n}$ (as $n = 1$ for the metal at $\mathbf{Z} < \mathbf{0}$ and $n = 2$ for dielectric at $\mathbf{Z} > \mathbf{0}$).
- **ω** indicates the wave's angular frequency.
- Both signs ± are + for the metal, − for the dielectric.
- $\boldsymbol{E_z}$, $\boldsymbol{E_x}$ are the z- and x- electric field vector components while, $\boldsymbol{H_y}$ is the y- magnetic field vector component, and the remaining components $(\boldsymbol{E_y}, \boldsymbol{H_x}, \boldsymbol{H_z})$ are all zero. That is to say, SPPs are transverse magnetic (TM) waves.
- The wave vector k is a complex vector, and the (x - components are real and the z - components are imaginary in the condition of a lossless SPP—the wave oscillates in the x direction and exponentially decreases in the z direction. For both materials, $\boldsymbol{K_x}$ is the same, although $\boldsymbol{K_{z,1}}$ is usually different($\boldsymbol{K_{z,2}}$).
- $\frac{\boldsymbol{H_0}}{\boldsymbol{E_0}} = -\frac{\varepsilon_1 \boldsymbol{\omega}}{\boldsymbol{K_{z,1}}\, \boldsymbol{C}}$ where ε_1 is the material permittivity 1 (for the metal), c is the vacuum light speed. This can be expressed as well explained below. $\frac{\boldsymbol{H_0}}{\boldsymbol{E_0}} = \frac{\varepsilon_2 \boldsymbol{\omega}}{\boldsymbol{K_{z,2}}\, \boldsymbol{C}}$

The following equations should also be held for the wave of this kind to satisfy the equations of Maxwell:

$$\frac{K_{z,1}}{\varepsilon_1} + \frac{K_{z,2}}{\varepsilon_2} = 0 \quad (4)$$

$$and \qquad {K^2}_x + {K^2}_{zn} = \varepsilon_n(\frac{\omega}{c})^2 \qquad n = 1,2 \tag{5}$$

The wave propagating over the surface has a dispersion relation is obtained by solving these two equations.

$$K_z = \frac{\omega}{c}\ (\frac{\varepsilon_1\,\varepsilon_2}{\varepsilon_1 + \varepsilon_2})^{1/2} \tag{6}$$

The metallic dielectric function in the electron gas's free electron model, which ignores attenuation, is

$$\varepsilon(\omega) = 1 - \frac{{\omega_p}^2}{\omega^2} \tag{7}$$

where the frequency of bulk plasma is

$$\omega_P = \sqrt{\frac{ne^2}{\varepsilon_0 m^*}} \tag{8}$$

Where **n** expresses the density of electron, **e** expresses the electron charge, **m∗** expresses electron effective mass and $\boldsymbol{\varepsilon_0}$ expresses the free-space permittivity. Fig.3 depicts the relation of dispersion. SPP operates like a photon at low $\boldsymbol{k}$, but as $\boldsymbol{k}$ rises, the relation of dispersion bends and reaches an asymptotic limit known as the "surface plasma frequency." Because the line of the light is to the dispersion curve right, $\boldsymbol{\omega = k \cdot c}$

The component that is out of plane of the SPP wave vector is totally imaginary and shows evanescent decay because the wavelength of the SPP is less than radiation in free-space. The asymptote of this curve is the frequency of surface plasma, which is determined by

$$\omega_{SP} = \omega_P/\sqrt{1 + \varepsilon_2} \tag{9}$$

In air case, the result is as follows:

$$\omega_{SP} = \omega_P/\sqrt{2} \tag{10}$$

If we suppose that ε_2 is real and $\varepsilon_2 > 0$, then $\varepsilon_1 < 0$, which is a criterion that metals satisfy, must be true. as a result of ohmic losses and interactions of electron-core, electromagnetic waves travelling through a metal are dampened as dielectric function imaginary component, these effects are observable. $\boldsymbol{\varepsilon_1 = \varepsilon_1' + i \cdot \varepsilon_1''}$ is the expression for the metal dielectric function, where $\boldsymbol{\varepsilon_1'}$ and $\boldsymbol{\varepsilon_1''}$ are the dielectric function's real and imaginary parts, accordingly. In General, $\boldsymbol{|\varepsilon_1'| >> \varepsilon_1''}$ as a result,

the wavenumber can be decomposed into its real and imaginary components as follows [17]:

$$k_x = k'_x + ik''_x = [\frac{\omega}{c}(\frac{\varepsilon'_1 \varepsilon_2}{\varepsilon'_1 + \varepsilon_2})^{1/2}] + i[\frac{\omega}{c}(\frac{\varepsilon'_1 \varepsilon_2}{\varepsilon'_1 + \varepsilon_2})^{3/2} \frac{\varepsilon''_1}{2(\varepsilon'_1)^2}] \quad (11)$$

The wave vector provides information about the electromagnetic wave's physical features, as its spatial extent and wave vector matching coupling requirements.

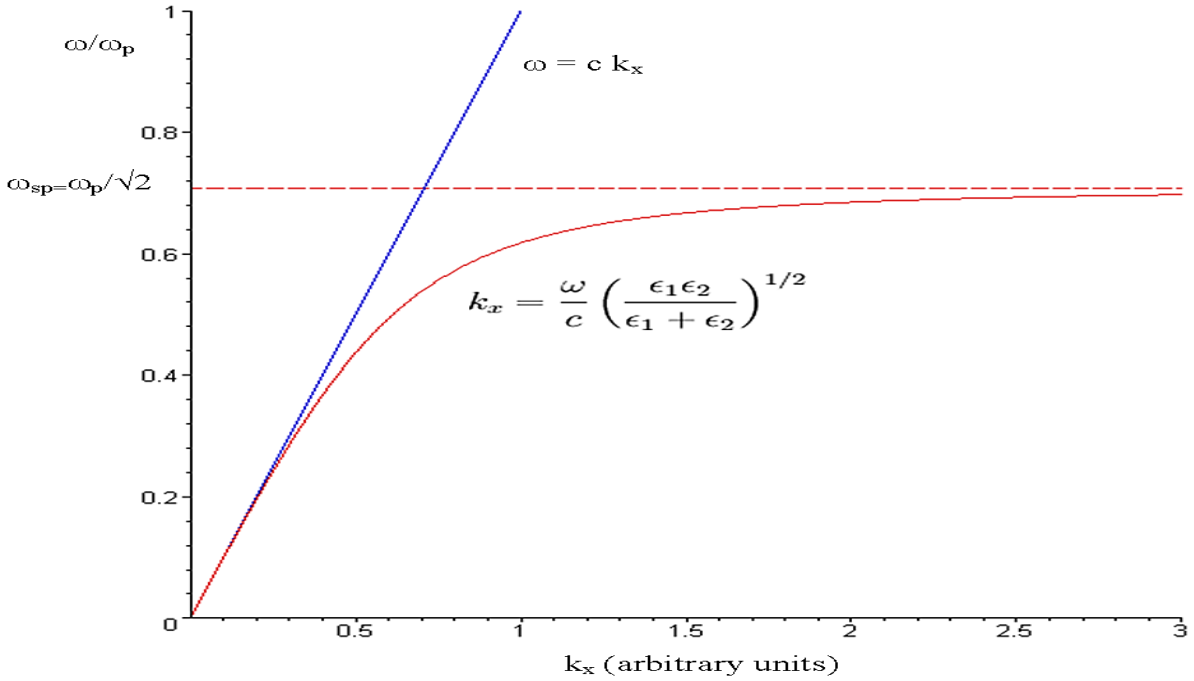

Fig.3: Surface plasmon polaritons' lossless dispersion curve. At low k, the curve of the surface plasmon [red] approaches the curve of the photon [blue].

3.2 Propagation Length and Skin Depth of SPP

Due to absorption, SPP loses energy to the metal as it propagates along the surface. Because with the electric field square, the surface plasmon intensity decreases, by the factor of $\exp\{-2k''_x x\}$, the intensity has reduced at a distance x. propagation length is the distance required for SPP intensity to be decreased by 1/e. This requirement is fulfilled at a length [23].

$$L = \frac{1}{2k''_x} \quad (12)$$

Therefore, electric field evanescently drops in perpendicular position to the metal's surface. The skin depth formula is widely used to approximate the depth of SPP

penetration through metal at low frequencies. In dielectric, the field would drop considerably very slowly. The decay lengths inside a metal and a dielectric medium could be represented as [23].

$$z_i = \frac{\lambda}{2\pi} \left(\frac{|\varepsilon'_1| + \varepsilon_2}{\varepsilon_i^2}\right)^{1/2} \quad (13)$$

Where the propagation medium is denoted by i . SPPs are typically employed to explore in homogeneities of a surface since they are particularly sensitive to minor alterations in the depth of the skin. As they have a lot of free electrons [24], metals are the only plasmonic substances available in visible and near-infrared light, resulting in a high plasma frequency.

Metals, Regrettably, they suffer from ohmic losses, which able to reduce plasmonic device performance. The demand for decreased loss has sparked research towards producing alternative plasmonic materials [24-26].

The optical performance is influenced by both the loss and polarization of the material. For a SPP, the factor of quality Q_{SPP} is defined as $\frac{\varepsilon'^2}{\varepsilon''}$ [26]. The quality factors and propagation lengths of SPP of four main plasmonic metals: Al, Ag, Au and Cu under perfect circumstances, deposited as a result of thermal evaporation are shown in the table below [27]. The films of Al, Ag, Au, and Cu have optical data were used to calculate the propagation lengths and quality factors of SPP.

Table 2 SPP propagation lengths and quality factors for four common plasmonic metals

Wavelength Regime	Metal	$Q_{SPP}(\times 10^{-3})$	$L_{SPP}(\mu m)$
Ultraviolet (280 nm)	Al	0.07	2.5
Visible (650 nm)	Ag	1.2	84
	Cu	0.42	24
	Au	0.4	20
Near-Infrared (1000 nm)	Ag	2.2	340
	Cu	1.1	190
	Au	1.1	190
Telecom (1550 nm)	Ag	5	1200
	Cu	3.4	820
	Au	3.2	730

For the visible, near-infrared (NIR), as well as wavelengths of telecom, silver has the lowest losses of any contemporary material [27].

For the visible as well as near-infrared, copper and gold are nearly identical, For the wavelengths of telecom, copper has a little advantage. Gold is distinguished from silver and copper that in natural conditions it has the Feature of being chemically stable, this makes it perfect for plasmonic biosensors [28]. In the UV range (< 330 nm), aluminum, along with copper, is the best plasmonic material and is also CMOS compatible.

4. Results and Discussion

Noble metals offer a variety of characteristics that make them appropriate for plasmonic applications. Noble metal nanoparticles are distinguished by the presence of absorption bands in the optical spectrum range, which are formed by resonance plasmon excitation. Aluminum is a versatile metal with a multitude of benefits, including corrosion resistance, electrical and thermal conductivity, reflectivity, ductility, odorless, low cost, impermeability, and recyclability. It is well-known for being both light and adaptable. It may also be cast, melted, formed, machined, and extruded, allowing it to be made into a selection of shapes and then fabricated to fit applications wide range. Metals having different attributes are necessary for plasmonic interactions to happen. When light interacts with resonant nanostructures in the interface of the metal-dielectric, SPPs are generated. Metal, rather than dielectric, plays a larger role in plasmonic applications due to its electrical and optical characteristics that are unique coming from the huge number of electrons available for free. The use of nanostructured metals rather than bulk metals in plasmonics is the most significant sign. SPPs made of gold and aluminum have excellent light trapping capabilities, as well as increased IQE and responsivity. It is provided a 2-D simulation of the PIN photodetector's most important properties, as well as the improvement with gold and aluminum SPPs, in this paper. Because SPPs are practically free-electron performance, in noble metals, they can be excited effectively. with nanostructures. The nanotextured noble metal systems contain superior characteristics for generating localized high-density energy areas and show higher betterment of exceptional optical absorption (EOA). Photolithography and near-field microscopy both benefit from this effect and its underlying process [29]. Periodic nanostructures may efficiently produce light transmission and Surface plasmons (SPs) are a fascinating device type because of their ability to absorb light

as well as their potential usage in optical communication networks. A typical MSM-PD is a symmetric device made up of two diodes with Schottky type that are coupled back-to-back on the substrate of the semiconductor [30]. GaAs is a semiconductor which has a direct bandgap that absorbs and retransmits photons more efficiently than indirect semiconductors such as Ge and Si [31]. The PIN photodetector's operating parameters: IQE (Internal quantum efficiency) can be calculated by [32]:

$$\mathbf{IQE} = \frac{\boldsymbol{I_P}}{\boldsymbol{P_{in}}} . \frac{\boldsymbol{hc}}{\boldsymbol{\lambda . e}} \tag{14}$$

The photocurrent (I_P)-to-input power (P_{in}) ratio is used to calculate responsivity (R) [33].

$\boldsymbol{R} = \frac{\boldsymbol{I_P}}{\boldsymbol{P_{in}}}$ The photocurrent can be defined as [34]:

$$(\boldsymbol{I_P}) = \boldsymbol{IQE} . \boldsymbol{e} \left(\frac{\boldsymbol{P_{opt}}}{\boldsymbol{h} . \boldsymbol{\nu}}\right) \tag{15}$$

$\boldsymbol{P_{opt}}$ expresses the optical power, and h expresses the constant of Planck, where **e** expresses the elementary electron charge. Photocurrent is an electric current created in a photodetector by incident light [35]. Depending on the light wavelength and nanostructure geometry, many metal nanostructures, Subwavelength slits, for example, exhibit plasmonic effects and can generate a high-intensity zone. In the bonds, all visible spectrum frequencies are absorbed and can pass across the metal via electron transfer due to their electron states that are not full When lighted, nearly all of energy of the metals is reflected at same incident wavelength, while light which is absorbed liberated by free electrons in the nearby area, giving the metal luster or sparkling appearance [36].

In most instances, each absorbed photon produces just one photoelectron. As evaluated by the quantum efficiency of a photodiode, some of carriers are produced only if they contribute to photocurrent in a weak proportion. and so be lost. In photovoltaic mode, in other words, when the bias voltage is set to zero, the quantum efficiency is not significantly decreased, and some forward voltage is needed to considerably lower the photocurrent. As a result, the bias voltage has a minor impact on the responsivity. Until a certain level of saturation is reached, the photocurrent in many detectors over several decades, is nearly proportional to the incident intensity or power in optics [37].

4.1 PIN photodetector simulation results

This part summarizes the results of the simulation for the proposed PIN photodetector, with comprehensive details on the output data shown in Figs. 4, 5,

6,7 and Table 3, as seen in Fig. 4, (Internal Quantum Efficiency) IQE curves for the various grating shapes such as rectangular, triangular, ellipse, circle and bowtie. IQE of the Au SPP rectangle grating was 85%, whereas the IQE of the Au and Al SPP circle grating is 82.30 %, which is less efficient than the prior model. IQE of the Au and Al SPP ellipse grating is 87.06 %, which was a slight enhancement over the two prior models. While the IQE of Au and Al SPP triangle grating reached 94.48 %, with an additional 9.48% increase. and also, in the case of Au and Al SPP rectangle grating the IQE is 95.01%. The higher outcome in this proposed study is for Au and Al SPP bowtie grating, which has an IQE of 98.48% with a total enhancement IQE of 13.48% among the first and last models. Also, in the curves of current shown in Fig.5, there is a noticeable enhancement also appeared significantly in the case of Au and Al SPP bowtie grating, As the output current in this case is 3.65 uA, While the output current is 1.40 uA in the first model of Au SPP rectangle grating .The effect of these various shapes of gratings on responsivity is also studied as depicted in Fig. 6 and it is found that the best result of responsivity for Au and Al SPP bowtie grating responsivity is 36.45 A/W, while the first model of Au SPP rectangle grating responsivity is 14 A/W. Moreover, the electric field intensity of the two models with Au SPP rectangle grating and with Au and Al SPP bowtie grating indicated in Fig.7, More enhancement at the case of Au and Al SPP bowtie grating in the proposed PIN photodetector.

Table 3 values of PIN photodetector simulation results

Grating Shapes	**IQE [%]**	**Photocurrent [uA]**	**Responsivity [A/W]**
Au and Al SPP Bowtie grating	98.48	3.65	36.45
Au and Al SPP Rectangle grating	95.01	1.70	17.01
Au and Al SPP Triangle grating	94.48	1.69	16.97
Au and Al SPP Ellipse grating	87.06	1.50	15.04
Au and Al SPP Circle grating	82.30	1.25	12.52
Au SPP Rectangle grating [36]	85.00	1.40	14.00

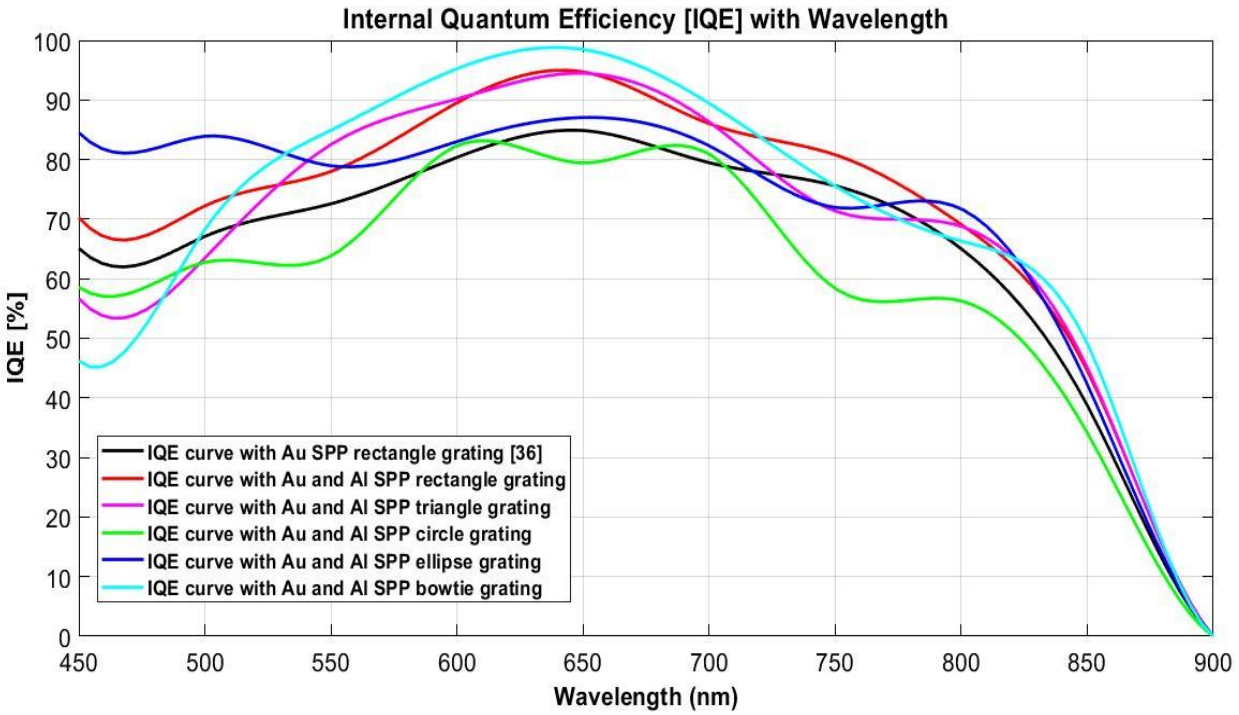

Fig.4 Internal Quantum Efficiency [IQE] versus wavelength (nm) of proposed PIN photodetector with various shapes of grating surface. The simulation was run under these circumstances: $1*10^{21}$ atoms$/cm^3$ doping of gallium arsenide and 2 V voltage bias.

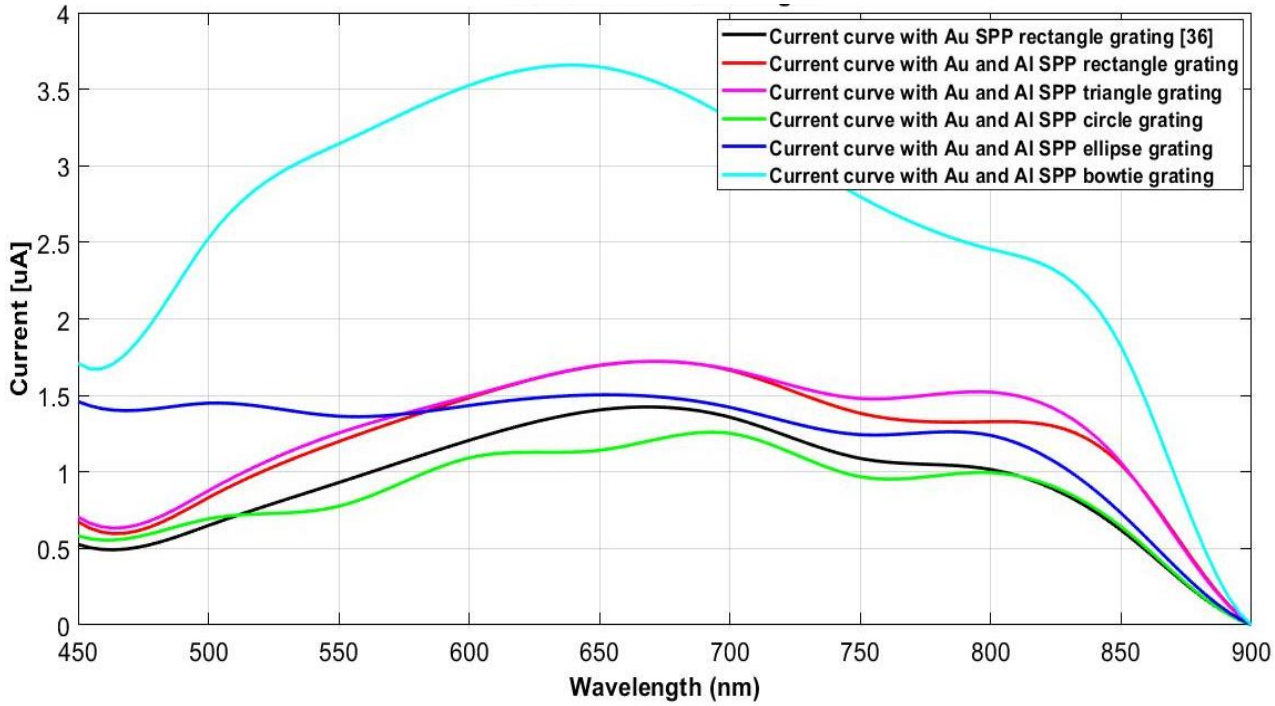

Fig.5: Current curve of proposed PIN photodetector versus wavelength with varying shapes of grating surface.

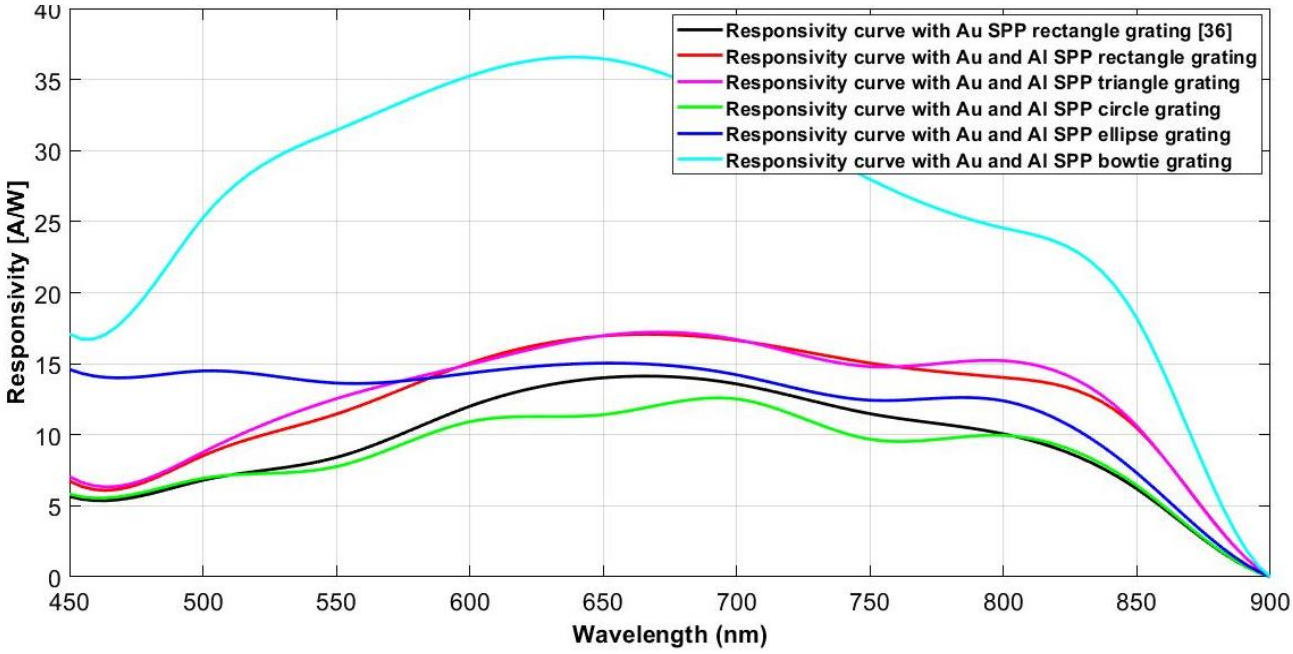

Fig.6 Responsivity curve with wavelength of the modelled PIN GaAs photodetector with different grating shapes

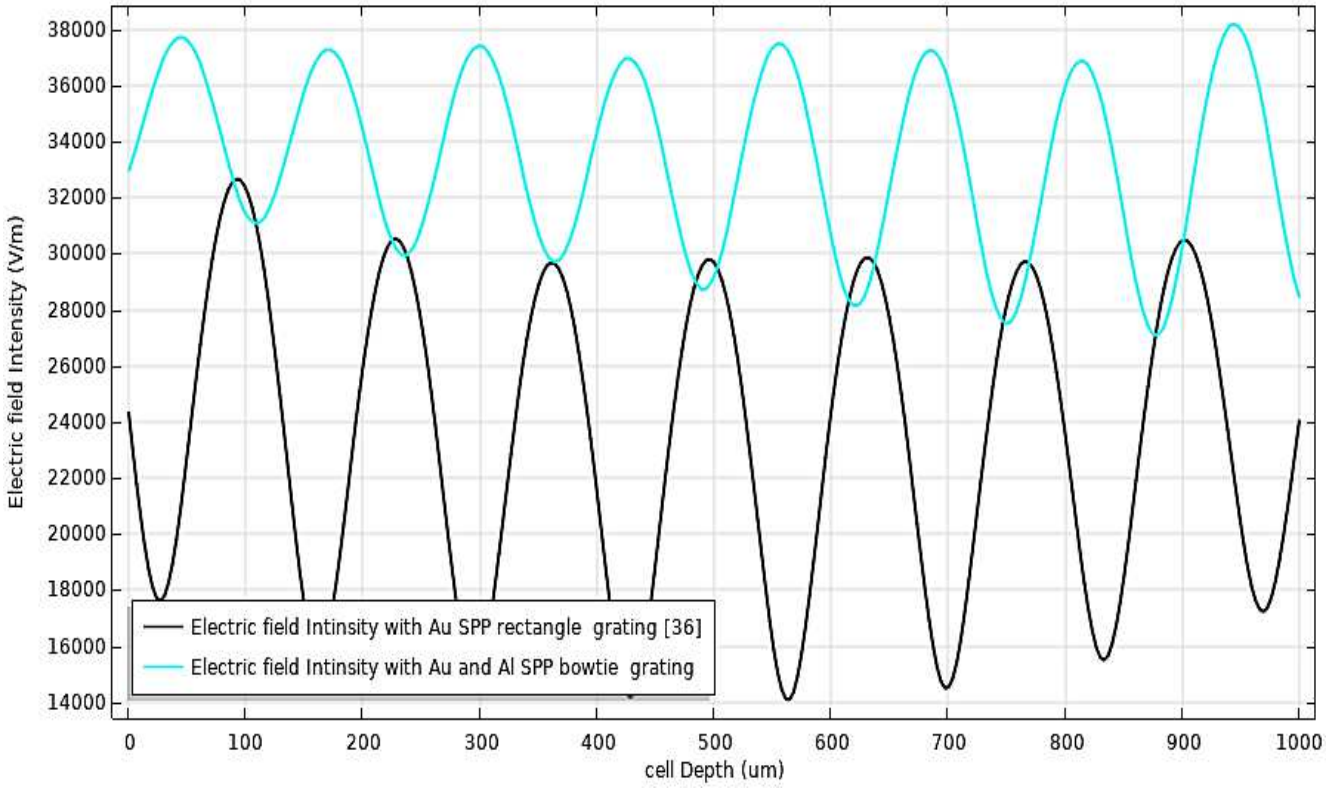

Fig.7: Electric Field Intensity curve with Cell Depth of the modelled PIN Photodetector with Au SPP rectangle grating and with Au and Al bowtie grating.

4.2 Effect of Bowtie grating with different gap sizes on PIN photodetector performance

This section shows the results obtained when using the bowtie grating with different gaps between the two triangles in the model design under the same conditions of the proposed PIN photodetector. The gap sizes used are 30 nm, 50 nm, 70 nm, 100 nm as in **Fig**.8, and also in the case that the two triangles are tangent without a gap between them. We found that the greater the size of the gap, the lower the performance of the photodetector. As depicted in **Fig**. 9, the internal quantum efficiency in the case of the bowtie grating with a gap size 100 nm is 91.64, while the IQE of the bowtie grating with a gap size 70 nm is 93.54 a slight enhancement over the previous case. When the gap size is 50 nm, the IQE is 94.83, Also When the gap size is 30 nm, the IQE is 96.27. There has been more enhancement than in previous instances. The higher IQE obtained in the case of the bowtie without a gap between the two triangles as the IQE is 98.48. In addition, in the current curves shown in **Fig.** 10, there is a noticeable enhancement in the case of bowtie grating without a gap between the two triangles, as the output current in this instance is 3.65 uA, whereas the output current in the case of bowtie grating with a gap size 100 nm is 3.39 uA. Bowtie grating with different gap sizes also has effect on responsivity of the proposed PIN photodetector as seen in **Fig.** 11, as the responsivity of the bowtie grating with a gap size 100 nm is 33.92 A/W, however in the case of the bowtie grating without a gap between the two triangles is 36.45 A/W.

Table 4: Values of PIN photodetector simulation results with different bowtie grating gap sizes

Bowtie grating gap sizes	IQE [%]	Photocurrent [uA]	Responsivity [A/W]
Bowtie grating without a gap between the two triangles	98.48	3.65	36.45
bowtie grating with a gap size 30 nm	96.27	3.56	35.63
bowtie grating with a gap size 50 nm	94.83	3.51	35.10
bowtie grating with a gap size 70 nm	93.54	3.46	34.63
bowtie grating with a gap size 100 nm	91.64	3.39	33.92

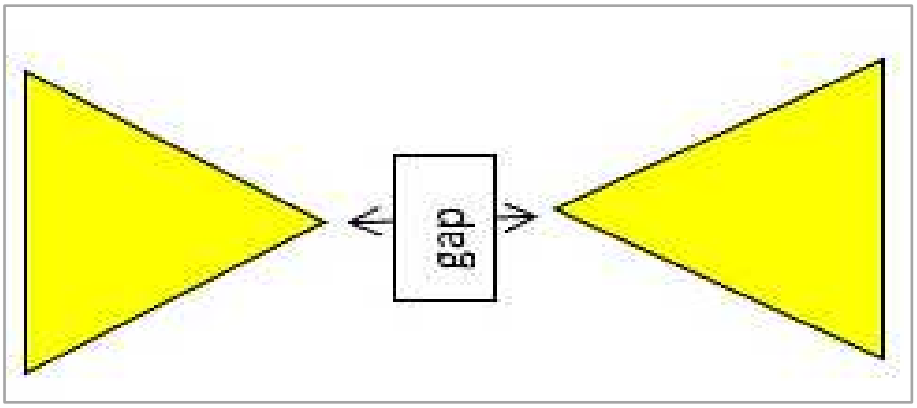

Fig.8 Diagrammatic depiction of the bowtie grating with a gap between the two triangles of size 30, 50, 70 and 100 nm.

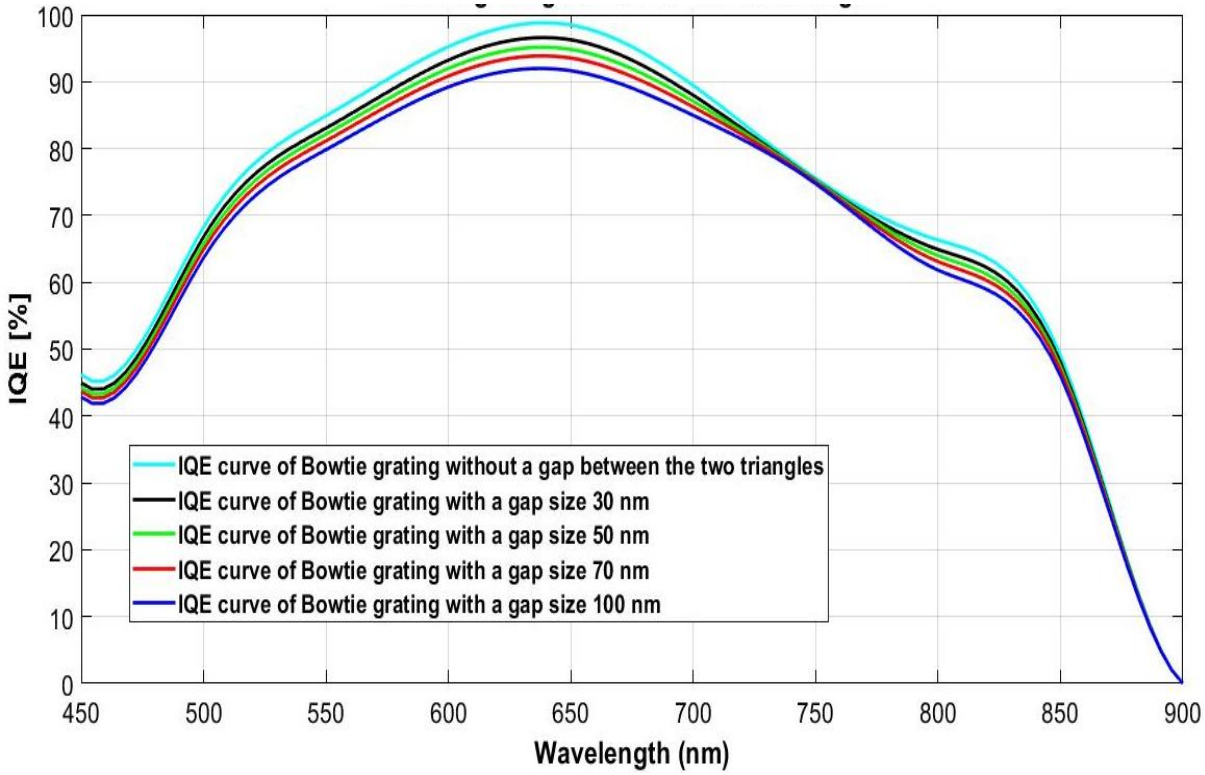

Fig.9: Internal Quantum Efficiency curve with wavelength of the modelled PIN Photodetector with different bowtie grating gap sizes.

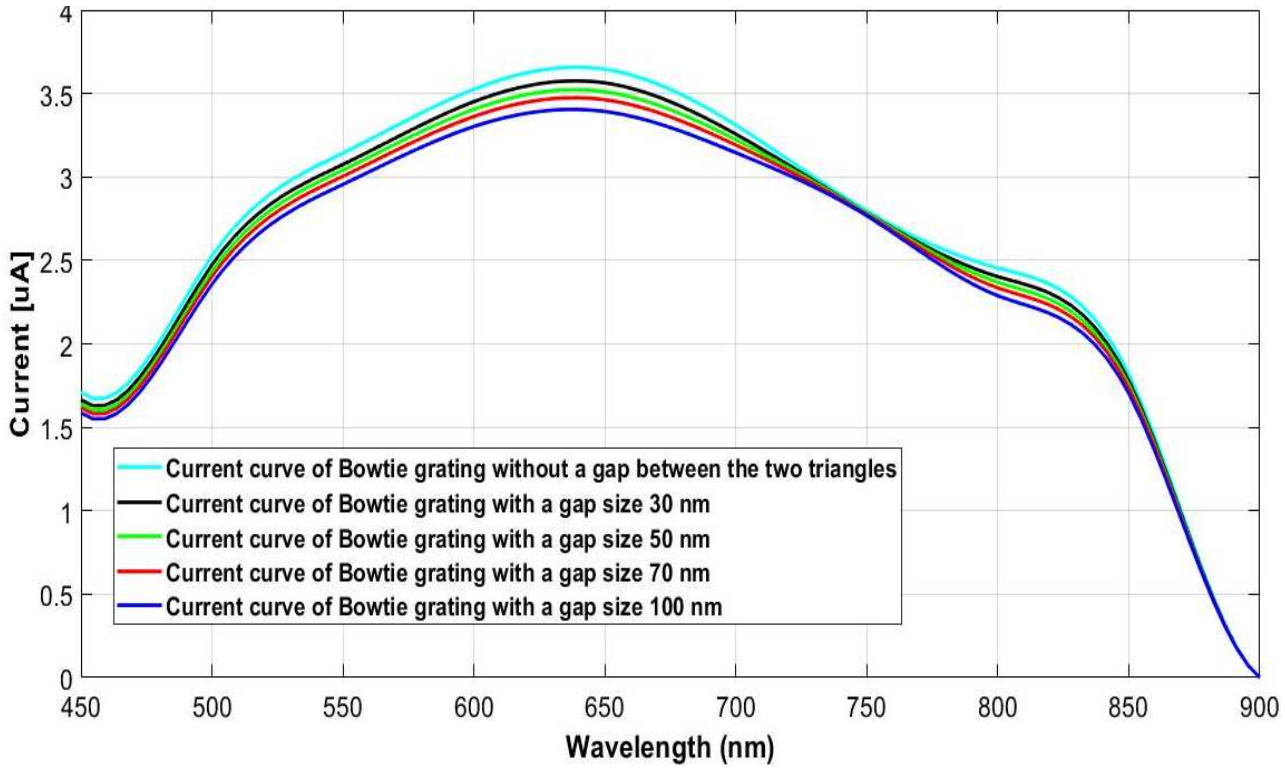

Fig.10: Current curve with wavelength with various gap sizes of bowtie grating.

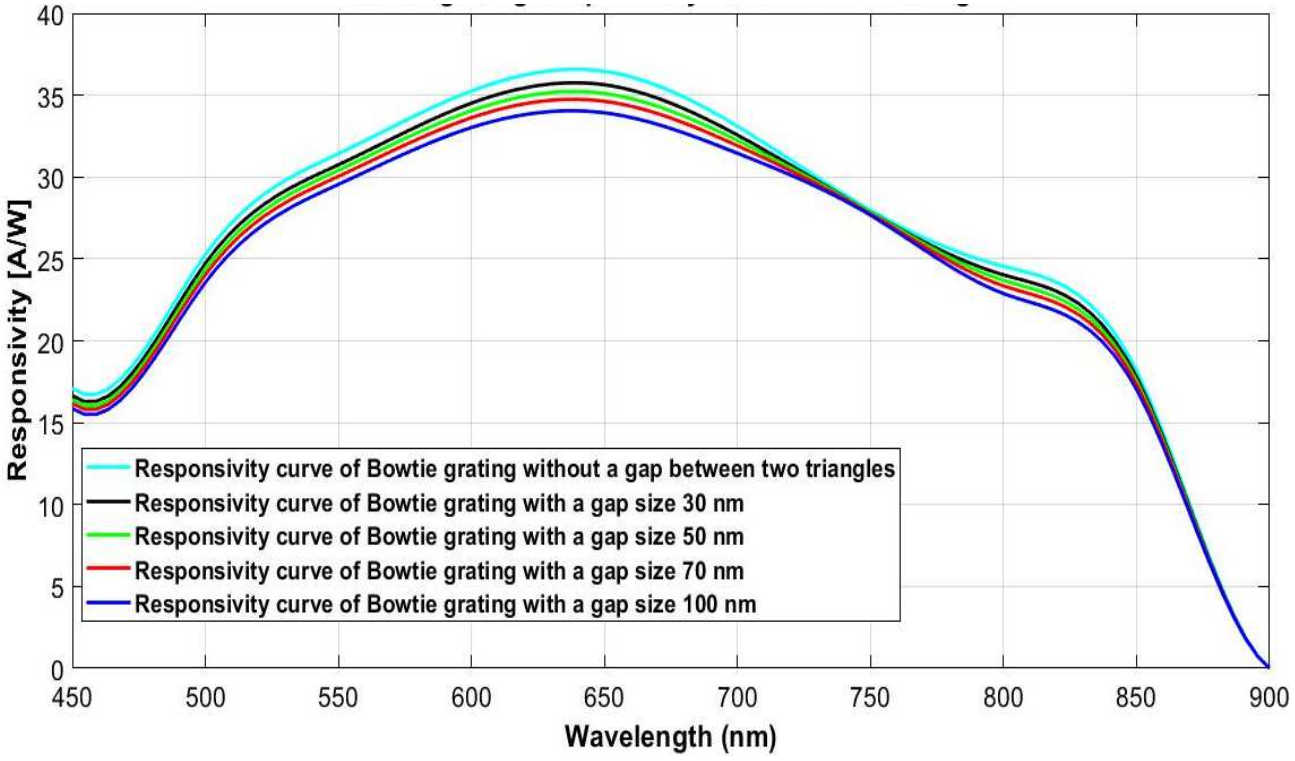

Fig.11 Responsivity curve with wavelength of the modelled PIN GaAs photodetector with different bowtie grating gap sizes

5. Conclusion

Plasmonics is interesting because structures made of metal can restrict light by connecting a carrier electromagnetic wave with a charge oscillation at metal's surface. These oscillations have a wavelength that is significantly lower than the corresponding wavelength of light in space. It is feasible to develop ultra-compact devices with greater speed by allowing for subwavelength-scale light–matter interaction. It is demonstrated in this paper how to construct a photodetector with a PIN type using the SPP (surface plasmon polariton) technique. The SPP layers in the modelled photodetector with a GaAs PIN type are gold and aluminum. Where by adding aluminum and using it with gold as just a SPP layers on the photodetector surface, this led to an increase in IQE (Internal Quantum Efficiency). Also, it is presented a proposed design for gold (Au) and aluminum (Al) SPP PIN photodetector with various grating shapes like rectangular, triangular, ellipse, circle and bowtie. It is found that the design of (Au) and (Al) SPP PIN photodetector with bowtie grating achieve higher IQE up to 98.48%. In addition, the Au and Al SPP design of the photodetector with bowtie grating remarkably improves photocurrent and responsivity. It is also studied the effect of bowtie grating with different gap sizes between the two triangles on the performance of the proposed PIN photodetector. Through this study, it is found that the greater the gap size between the two triangles in the bowtie grating model, the lower the performance of the photodetector, as in the case of the bowtie grating without a gap between the two triangles, IQE is 98.48%, while IQE decreased to 91.64% in the case of bowtie grating with a gap size 100 nm, as well as output current and responsivity have decreased by increasing the gap size.

Statements and Declarations

Funding: No funds, grants, or other support were received during the preparation of this paper

Competing Interests: The authors declare that there is no confict of interest regarding the manuscript.

Data Availability: All data is available and will be provided upon request by the corresponding author.

Author Contributions: *All authors contributed to the study conception and design. Material preparation, data collection analysis*, prototype design model, simulation and results interpretation were *performed by [Nada AbdElaziz], [*Bedir Yousif*]* ,[*Eman*

AbdElhalim],[*Waleed M. Gaballah*] *and [Ahmed S. Samra]. The first draft of the manuscript was written by [*Nada AbdElaziz*], [*Bedir Yousif*] and all authors commented on previous versions of the manuscript. All authors read and approved the final manuscript."*

Ethics approval: *This study no ethical approval is required.*

Consent to participate: *Not Applicable*

Consent to publish: *Not Applicable*

6. References

1. Chen, H., Liu, H., Zhang, Z., Hu, K., & Fang, X. (2016). Nanostructured photodetectors: from ultraviolet to terahertz. *Advanced Materials*, *28*(3), 403-433.
2. Maier, S. A., Brongersma, M. L., Kik, P. G., Meltzer, S., Requicha, A. A., & Atwater, H. A. (2001). Plasmonics—a route to nanoscale optical devices. Advanced materials, 13(19), 1501-1505.
3. Lai, Y. S., Tsai, C. Y., Chang, C. K., Huang, C. Y., Hsiao, V. K., & Su, Y. O. (2016). Photothermoelectric effects in nanoporous silicon. Advanced Materials, 28(13), 2644-2648.
4. Hössbacher, C., Salamin, Y., Fedoryshyn, Y., Heni, W., Bäuerle, B., Josten, A., & Leuthold, J. (2017). Optical interconnect solution with plasmonic modulator and Ge photodetector array. IEEE Photonics Technology Letters, 29(21), 1760-1763.
5. Wang, F., & Melosh, N. A. (2011). Plasmonic energy collection through hot carrier extraction. Nano letters, 11(12), 5426-5430.
6. Chalabi, H., Schoen, D., & Brongersma, M. L. (2014). Hot-electron photodetection with a plasmonic nanostripe antenna. Nano letters, 14(3), 1374-1380.
7. Li, W., Coppens, Z. J., Besteiro, L. V., Wang, W., Govorov, A. O., & Valentine, J. (2015). Circularly polarized light detection with hot electrons in chiral plasmonic metamaterials. Nature communications, 6(1), 1-7.
8. Brongersma, M. L. (2016). Plasmonic photodetectors, photovoltaics, and hot-electron devices. Proceedings of the IEEE, 104(12), 2349-2361.

9. Atwater, H. A., & Polman, A. (2011). Plasmonics for improved photovoltaic devices. Materials for sustainable energy: a collection of peer-reviewed research and review articles from Nature Publishing Group, 1-11.
10. Schuller, J. A., Barnard, E. S., Cai, W., & Jun, Y. C. (2010). 1. S. White and ML Brongersma. Nat. Mater, 9, 193-204.
11. Hyun, J. K., & Lauhon, L. J. (2011). Spatially resolved plasmonically enhanced photocurrent from Au nanoparticles on a Si nanowire. Nano letters, 11(7), 2731-2734.
12. Zheng, B. Y., Wang, Y., Nordlander, P., & Halas, N. J. (2014). Color-selective and CMOS-compatible photodetection based on aluminum plasmonics. Advanced Materials, 26(36), 6318-6323.
13. Shautsova, V., Sidiropoulos, T., Xiao, X., Güsken, N. A., Black, N. C., Gilbertson, A. M., ... & Oulton, R. F. (2018). Plasmon induced thermoelectric effect in graphene. Nature communications, 9(1), 1-9.
14. Liu, Y., Cheng, R., Liao, L., Zhou, H., Bai, J., Liu, G.,& Duan, X. (2011). Plasmon resonance enhanced multicolour photodetection by graphene. Nature communications, 2(1), 1-7.
15. Wu, D., Yan, K., Zhou, Y., Wang, H., Lin, L., Peng, H., & Liu, Z. (2013). Plasmon-enhanced photothermoelectric conversion in chemical vapor deposited graphene p–n junctions. Journal of the American Chemical Society, 135(30), 10926-10929.
16. Steen, W. M. (2000). Principles of Optics M. Born and E. Wolf, 7th (expanded) edition, Cambridge University Press, Cambridge, 1999, 952pp.@ $37.50/US $59.95, ISBN 0-521-64222-1. Optics and Laser Technology, 5(32), 385.
17. Raether, H. (1988). Surface plasmons on smooth surfaces. In Surface plasmons on smooth and rough surfaces and on gratings (pp. 4-39). Springer, Berlin, Heidelberg.
18. Gramotnev, D. K., & Bozhevolnyi, S. I. (2010). Plasmonics beyond the Diffraction Limit. Nature Photonics, 4, 83-91.
19. Rohizat, N. S., Ripain, A. H. A., Lim, C. S., Tan, C. L., & Zakaria, R. (2021). Plasmon-enhanced reduced graphene oxide photodetector with monometallic of Au and Ag nanoparticles at VIS–NIR region. Scientific reports, 11(1), 1-10.
20. Bashevoy, M. V., Jonsson, F., Krasavin, A. V., Zheludev, N. I., Chen, Y., & Stockman, M. I. (2006). Generation of traveling surface plasmon waves by free-electron impact. Nano letters, 6(6), 1113-1115.

21. Zeng, S., Yu, X., Law, W. C., Zhang, Y., Hu, R., Dinh, X. Q., ... & Yong, K. T. (2013). Size dependence of Au NP-enhanced surface plasmon resonance based on differential phase measurement. Sensors and Actuators B: Chemical, 176, 1128-1133.
22. Cottam, M. G., & Tilley, D. R. (2019). Introduction to surface and superlattice excitations. CRC Press.
23. Homola, J., & Piliarik, M. (2006). Surface plasmon resonance (SPR) sensors. In Surface plasmon resonance based sensors (pp. 45-67). Springer, Berlin, Heidelberg.
24. West, P. R., Ishii, S., Naik, G. V., Emani, N. K., Shalaev, V. M., & Boltasseva, A. (2010). Searching for better plasmonic materials. Laser & photonics reviews, 4(6), 795-808.
25. Boltasseva, A., & Atwater, H. A. (2011). Low-loss plasmonic metamaterials. Science, 331(6015), 290-291.
26. Blaber, M. G., Arnold, M. D., & Ford, M. J. (2010). A review of the optical properties of alloys and intermetallics for plasmonics. Journal of Physics: Condensed Matter, 22(14), 143201.
27. McPeak, K. M., Jayanti, S. V., Kress, S. J., Meyer, S., Iotti, S., Rossinelli, A., & Norris, D. J. (2015). Plasmonic films can easily be better: rules and recipes. ACS photonics, 2(3), 326-333.
28. Homola, J. (2003). Present and future of surface plasmon resonance biosensors. Analytical and bioanalytical chemistry, 377(3), 528-539.
29. Das, N., Karar, A., Vasiliev, M., Tan, C. L., Alameh, K., & Lee, Y. T. (2011). Analysis of nano-grating-assisted light absorption enhancement in metal–semiconductor–metal photodetectors patterned using focused ion-beam lithography. Optics Communications, 284(6), 1694-1700.
30. Das, N., Masouleh, F. F., & Mashayekhi, H. R. (2013). A Comprehensive Analysis of Plasmonics-Based GaAs MSM-Photodetector for High Bandwidth-Product Responsivity. Advances in OptoElectronics.
31. Ozbay, E. (2006). Plasmonics: merging photonics and electronics at nanoscale dimensions. science, 311(5758), 189-193.
32. Salamin, Y., Ma, P., Baeuerle, B., Emboras, A., Fedoryshyn, Y., Heni, W., & Leuthold, J. (2018). 100 GHz plasmonic photodetector. ACS photonics, 5(8), 3291-3297.
33. Zhao, X., Moeen, M., Toprak, M. S., Wang, G., Luo, J., Ke, X., & Radamson, H. H. (2020). Design impact on the performance of Ge PIN

photodetectors. Journal of Materials Science: Materials in Electronics, 31(1), 18-25.
34. Karelits, M., Mandelbaum, Y., Chelly, A., & Karsenty, A. (2018). Laser beam scanning using near-field scanning optical microscopy nanoscale silicon-based photodetector. Journal of Nanophotonics, 12(3), 036002.
35. Gay, G., Alloschery, O., De Lesegno, B. V., Weiner, J., & Lezec, H. J. (2006). Surface wave generation and propagation on metallic subwavelength structures measured by far-field interferometry. Physical review letters, 96(21), 213901.
36. Yousif, B., Abo-Elsoud, M. E. A., & Marouf, H. (2020). High-performance enhancement of a GaAs photodetector using a plasmonic grating. Plasmonics, 15(5), 1377-1387.
37. Dionne, J. A., Lezec, H. J., & Atwater, H. A. (2006). Highly confined photon transport in subwavelength metallic slot waveguides. Nano letters, 6(9), 1928-1932.